Zuo *et al. Biological Procedures Online* (2026) 28:26
https://doi.org/10.1186/s12575-026-00341-5

Biological Procedures Online

RESEARCH Open Access

Integrated Genomic and Single-Cell Analysis Identifies Notch1 as a Metastasis Suppressor in Nasopharyngeal Carcinoma Targeted by the AKT/Smad3 Axis

Jingjing Zuo[1†], Shiyong Huang[1†], Mengyuan Dai[2], Fen Li[1,3], Ting Huang[4], Lei Wang[1], Chenglin Qi[5], Zezhang Tao[1,3*] and Linfeng Ye[4*]

Abstract

Background Notch1 exhibits a high mutation rate in head and neck squamous cell carcinoma (HNSCC), but its functional role in nasopharyngeal carcinoma (NPC) invasion and metastasis remains incompletely understood. This study systematically investigates the function and molecular mechanisms of Notch1 as a metastatic suppressor in NPC.

Methods Notch1 expression levels were assessed in NPC tissue microarrays using immunohistochemistry, and correlations with tumor differentiation and metastasis were analyzed. TCGA databases were mined to explore mutation rates and sample clustering based on EMT-related gene signatures. Integrated analysis of TCGA and GEO datasets identified Notch1-associated genes, enabling molecular classification of patients. Additionally, scRNA-seq of NPC clinical samples was performed to validate the association between Notch1, stemness, and EMT features in the tumor microenvironment. The biological functions of Notch1 were further examined in vitro using proliferation (CCK-8, colony formation), migration and invasion (Transwell, wound healing) assays, as well as in vivo xenograft and metastatic models. Molecular mechanisms were probed by examining EMT markers, Smad3 phosphorylation and nuclear translocation, and protein-protein interactions via co-immunoprecipitation.

Results Immunohistochemistry revealed significantly reduced Notch1 expression in NPC tissues, closely associated with poor differentiation and lymph node metastasis. TCGA analysis showed a 16.8% Notch1 mutation rate in HNSCC. Consensus clustering based on EMT-related genes identified subgroups with significant differences in Notch1 mutation status. Using 181 Notch1-related genes from integrated datasets, patients were further classified into three molecular subtypes (C1, C2, C3) with distinct prognosis, Notch1 mutation rates, EMT status, immune landscapes, and ferroptosis-related gene expression. Notably, the C2 subgroup exhibited the highest Notch1 mutation rate, enhanced

†Jingjing Zuo and Shiyong Huang contributed equally to this work.

*Correspondence:
Zezhang Tao
rm001983@whu.edu.cn
Linfeng Ye
13627113032@163.com

Full list of author information is available at the end of the article

EMT, poorest prognosis, and immune suppression.Consistent with these multidimensional datasets, scRNA-seq analysis of primary NPC samples showed that Notch1-high tumor cells preferentially retained a differentiated epithelial, low-EMT/low-stemness phenotype, further supporting an EMT- and metastasis-suppressive role of Notch1 in clinical tumors. Functionally, Notch1 was downregulated across multiple NPC cell lines; knockout of Notch1 significantly promoted NPC cell proliferation, migration, invasion, and EMT both in vitro and in nude mouse models. Mechanistically, Notch1 loss increased EMT marker expression, augmented Smad3 phosphorylation and nuclear translocation, all without altering total Smad3 levels. Notch1 intracellular domain was found to interact directly with Smad3, while AKT and Smad3 interaction decreased upon Notch1 depletion, resulting in elevated Smad3 phosphorylation and EMT gene activation.

Conclusions Notch1 suppresses EMT and metastasis in NPC through regulation of the AKT/Smad3 pathway. These findings provide novel insights for molecular classification and targeted treatment strategies in NPC.

Keywords Notch1, Molecular Subtyping, HNSCC, NPC, scRNA-seq, EMT, Smad3, AKT

Introduction

Nasopharyngeal carcinoma (NPC) is a malignant epithelial tumor with a distinct geographic and ethnic distribution, particularly prevalent in Southeast Asia and Southern China [1]. Despite advances in radiotherapy and chemotherapy, local recurrence and distant metastasis remain major challenges, underscoring the need to elucidate the molecular mechanisms governing NPC progression and metastasis [2].

The Notch signaling pathway plays a key role in cell fate determination, differentiation, and tissue homeostasis [3]. Among the Notch family members, Notch1 has garnered significant attention in cancer research due to its context-dependent dual roles in tumorigenesis [4, 5]. Notably, large-scale genomic studies have reported a high mutation frequency of Notch1 in HNSCC, with emerging evidence supporting its tumor-suppressive functions in various epithelial malignancies [4]. However, the exact role and molecular mechanisms of Notch1 in NPC invasion and metastasis remain insufficiently understood.

One of the central mechanisms driving cancer dissemination is EMT, a process characterized by the loss of epithelial features and acquisition of a mesenchymal phenotype, thereby endowing tumor cells with enhanced motility and invasive capacities [6, 7]. EMT is not only critical for metastasis, but also intimately linked with tumor plasticity, immune evasion, and resistance to therapy [8]. Nevertheless, the upstream regulatory networks and signaling crosstalk that control EMT activation in NPC require further clarification.

Accumulating evidence suggests that loss-of-function mutations or downregulation of Notch1 can promote oncogenic phenotypes through complex interactions with other signaling pathways, such as Wnt, Hedgehog, and TGF-β/Smad, as well as immune microenvironment remodeling [9]. Recent studies indicate a potential interplay between Notch1 and the Akt signaling axis, impacting both EMT progression and tumor–immune interactions [10]. However, direct molecular evidence delineating these mechanisms in NPC is lacking.

In this context, the present study systematically investigates the expression, mutation status, and clinical relevance of Notch1 in NPC using multi-omics bioinformatics, clinical tissue microarrays, and functional cellular and animal models. We further explore the molecular mechanisms underlying Notch1-mediated EMT regulation, with a particular focus on the Akt/Smad3 axis.

Our findings aim to elucidate the tumor-suppressive function of Notch1 in NPC, provide novel insights into molecular subtyping and therapeutic targeting, and offer a conceptual framework for understanding the complex cross-talk between signaling networks that drive NPC metastasis.

Materials and Methods

TCGA and GEO Samples

RNA sequencing expression data, gene mutation information, and related clinical data for head and neck squamous cell carcinoma (HNSCC) were downloaded from the TCGA database (https://portal.gdc.com). Mutation data were processed and visualized using the R package maftools to display the distribution of high-frequency mutated genes, including Notch1, in HNSCC. An epithelial-mesenchymal transition EMT-related gene set was employed for consensus clustering analysis of the TCGA-HNSCC cohort using the R package ConsensusClusterPlus. The maximum number of clusters was set to 6, with 80% of samples randomly resampled 100 times. The clustering algorithm was hierarchical clustering ("hc") with the "ward.D2" linkage method. Based on the clustering results, samples were stratified into distinct molecular subgroups. Subsequently, gene expression heatmaps were visualized using the R package pheatmap, including only genes with a variance greater than 0.1.

The GSE127770 dataset was utilized to identify Notch1-associated transcripts. This dataset comprises expression profiles of the SJG6 OSCC cell line, which

harbors a Notch1 truncating mutation. By performing differential expression analysis between the control group (Notch1-deficient) and the NICD-restored group (Notch1-active), we screened for DEGs using selection criteria of |log2FoldChange| > 1.3 and $P < 0.05$. Concurrently, HNSCC-related gene sets (RGS) were retrieved from GeneCards (Gifts score > 50, Relevance score > 5). The intersection of the Notch1-related DEGs and RGS yielded a Notch1-related gene set (NRGS, $n = 181$). Consensus clustering using these genes categorized patients into three subgroups: C1, C2, and C3.

Comparative analyses among these subgroups were conducted for multiple clinical and molecular features, including prognosis (Kaplan Meier survival curves and log-rank tests), clinical staging (N stage), Notch1 mutation status, stemness index, expression of ferroptosis-related genes, immune cell infiltration, and immune checkpoint molecules. The stemness index (mRNAsi) was calculated using the OCLR algorithm, with Spearman correlation coefficients applied to evaluate RNA expression correlation. The stemness index was normalized linearly to a range between 0 and 1. The ferroptosis gene set was derived from authoritative review literature. Immune cell type analysis was performed with the immunedeconv R package, while immune therapy response prediction was carried out using the TIDE algorithm (Tumor Immune Dysfunction and Exclusion). Differences in expression of immune-related genes, PI3K/AKT signaling components, and key EMT molecules were tested using appropriate statistical methods.

Correlation analysis two genes was performed using the R package ggstatsplot, applying Spearman correlation analysis, with $P < 0.05$ considered statistically significant.

scRNA-seq Data Analysis

To investigate the expression patterns and functional characteristics of Notch1 in the NPC tumor microenvironment at single-cell resolution, we obtained the raw scRNA-seq data from the GSE150825 dataset. This dataset comprises comprehensive single-cell transcriptomic profiles of 66,627 cells derived from 14 NPC patients.

Data processing and quality control: The raw gene expression matrix was processed using the Seurat R package (version 5.0). Quality control was strictly performed to filter out low-quality cells based on the following criteria: (1) cells expressing fewer than 200 genes or more than 6,000 genes; (2) cells with mitochondrial gene content exceeding 20%. After filtering, the data were normalized using the NormalizeData function, and the top 2,000 highly variable features were identified via FindVariableFeatures. To mitigate batch effects among different patients, the Harmony integration algorithm was applied. Principal Component Analysis (PCA) was performed for dimensionality reduction, followed by cell clustering using FindNeighbors and FindClusters (resolution = 0.5). The resulting clusters were visualized using Uniform Manifold Approximation and Projection (UMAP). Cell types were annotated based on the expression of canonical marker genes, including EPCAM (epithelial/tumor cells), PTPRC (immune cells), CD3D (T cells), CD79A (B cells), CD68 (myeloid cells), DCN (fibroblasts), and PECAM1 (endothelial cells).

Inferred Copy Number Variation (CNV) analysis: To distinguish malignant tumor cells from non-malignant epithelial cells, we inferred somatic copy number variations (CNVs) using the inferCNV R package. T cells from the same patient were used as the reference normal population. The analysis was performed with a cutoff of 0.1, and a dynamic threshold was applied for denoising.

Notch1-related functional analysis: Tumor cells were stratified into Notch1-High and Notch1-Low groups based on the median expression level of Notch1. Differential expression analysis was conducted using the FindMarkers function (Wilcoxon rank-sum test) to identify differentially expressed genes (DEGs) between the two groups. To evaluate the differentiation potential and stemness of tumor cells, we utilized the CytoTRACE algorithm. CytoTRACE scores were calculated to predict the developmental state of single cells, where a higher score indicates a less differentiated (more stem-like) state. Correlation analysis between Notch1 expression and CytoTRACE scores, as well as EMT markers (VIM, FN1), was performed using Spearman's rank correlation.

Table 1 Clinical data of NPC patients correlated with Notch1 expression

	Notch1 expression		Total	*P*-value
	Low ($n = 67$)	High ($n = 50$)		
Age, years				0.124
< 50	48	29	77	
≥ 50	19	21	40	
Sex				0.650
Male	52	37	89	
Female	15	14	28	
lymph node Metastasis				< 0.001
No	18	46	64	
Yes	49	4	53	

Tissue Samples

The tissue microarray (TMA) of NPC with detailed clinical characteristics and long-term follow-up data was obtained from Guilin Fanpu Biotech (Guilin, China, Nos. 1501 and 1502). A total of 117 NPCs were included in the TMA; 64 NPC tissue samples lacked cervical lymph node metastasis, while 53 NPC tissue samples had cervical lymph node metastasis. Anti-tumor therapy was

not administered to any of the patients prior to biopsy. An overview of the TMA is provided in (Table 1). The study on clinical tissue specimens was approved by the Medical Ethics Committee of Renmin Hospital of Wuhan University.

Cell Culture

Human NPC cell lines CNE-2, CNE-1, 6-10B, 5–8 F, C666-1, and HNE-1 were obtained from Guangxi Medical University. All cell lines were cultured in RPMI 1640 medium (HyClone; Life Sciences, USA) supplemented with 10% FBS (HyClone) at 37˚C, 5% CO2.

Generation of Notch1-Modified NPC Cell Lines via shRNA, CRISPR/Cas9 and Lentiviral Overexpression

For knockdown experiments, shNotch1 oligonucleotides were synthesized by Guangzhou Ruibo Co., Ltd., and NPC cells (6-10B, CNE-1) were transfected with 100 nM control siRNA or Notch1 shRNA using Lipofectamine 2000 according to the manufacturer's instructions. Transfection was carried out for 4–6 h on the day after plating, after which the medium was replaced with normal medium; cells were harvested 48 h post-transfection for protein extraction. For Notch1 knockout, a CRISPR/Cas9-targeted CNE-2 Notch1-/- stable cell line was constructed by Beijing Biocytogen Co., Ltd. (https://www.bbctg.com.cn/). Based on genomic analysis of CNE-2 cells, exons 6–21 of the Notch1 gene were replaced with antibiotic-resistant gene cassettes, which were selected by antibiotic titration and karyotyping. Cas9/sgRNA-mediated indels were also used to disrupt Notch1. The Notch1 coding sequence was divided into three fragments and synthesized into the Cas9 plasmid pTV-hNotch1 (puro) containing sgRNA; fragments 1, 2, and 3 were ligated into the TV-4G-EB vector using AIOTM. Cas9/sgRNA activity was evaluated with the Universal CRISPR Activity Assay (UCA), and Notch1 knockout cell lines were obtained by electroporation, drug selection, isolation of positive clones, sequencing, and expansion. For Notch1 overexpression, a lentiviral vector encoding Notch1 and GFP (Shanghai GeneChem Co., Ltd., Shanghai, China) was used to infect 6-10B cells (2 × 10^5 cells/well) at a multiplicity of infection (MOI) of 20; negative control (NC) cells were infected with control lentivirus. Stably transduced NPC cell lines (CNE-1, 6-10B, CNE-2, 5–8 F) were selected by culture for 1 week in complete medium (RPMI-1640 supplemented with 10% FBS, ampicillin, and kanamycin) containing puromycin (2 μg/ml).

Immunohistochemical Staining (IHC)

The two-step method was used for the immunohistochemical analysis of Notch1 expression. The slides were dried, dewaxed, and rehydrated in a gradient concentration of ethanol. The slides were pretreated with citrate buffer for antigen retrieval, and then immersed in 0.3% hydrogen peroxide to prevent endogenous peroxidase activity. Subsequently, incubated with primary antibody overnight at 4℃, Rinsed with PBS for 5 min, then incubated with secondary antibody (Poly-HRP Goat anti-rabbit; Maixin Biotech, China) for 30 min at room temperature. Dyed with 3, 3-diaminobenzidine (DBA) for 5 min, counterstained with Mayer's hematoxylin, dehydrated, and mounted.

CCK-8 Assay

After digestion, the cells were inoculated into 96-well plates at 2000 cells per well with five parallel holes in each group. After the cells adhered to the wall, the working medium was prepared with the CCK-8 reagent and culture medium at a ratio of 1:9. 100 μ l was added to each well instead of the original culture medium and incubated at 37 ℃ for 1 h. The absorbance (OD) was measured at the 450 nm wavelength of the enzyme labeling instrument. Taking the OD value on day 0 as the starting point, the OD value was measured every 24 h, and the cell growth curve was drawn.

Clonogenic Growth

Inoculate 400-1,000 cells/well per experimental group in 6-well plate culture plates. The culture was maintained for 14 days. After cloning, the cells were washed once with PBS, 1 ml of 4% paraformaldehyde was added to each well for 30 min, and washed once with PBS. Add 1 ml of crystal violet dye solution to each well and dye for 15 min. The cells were washed several times with PBS, allowed to dry, and photographed. To calculate the clonal formation rate, positive clones were observed under a microscope. Each clone had more than 50 cells, and the number of clones was quantified.

Confocal Immunofluorescence

Cells in the logarithmic growth phase were plated in a 24-well plate and crawled on slides overnight. The slides were washed with PBS and fixed with 4% paraformaldehyde (freshly prepared). The primary antibody was incubated overnight at 4 °C; the secondary antibody was incubated at room temperature for 1 h. After washing with PBS, a drop of 50% glycerol was dropped onto a clean glass slide, the lobes were removed from the slide onto the glycerol slide, and immunofluorescence laser confocal microscopy was used to observe the cells on the slide.

Western Blotting

The cells were harvested and lysed in buffer containing 1% Nonidet-P40, complete protease inhibitor cocktail (Roche), and 2 mM dithiothreitol. Lysates were resolved using 10% SDS-PAGE and transferred to PVDF

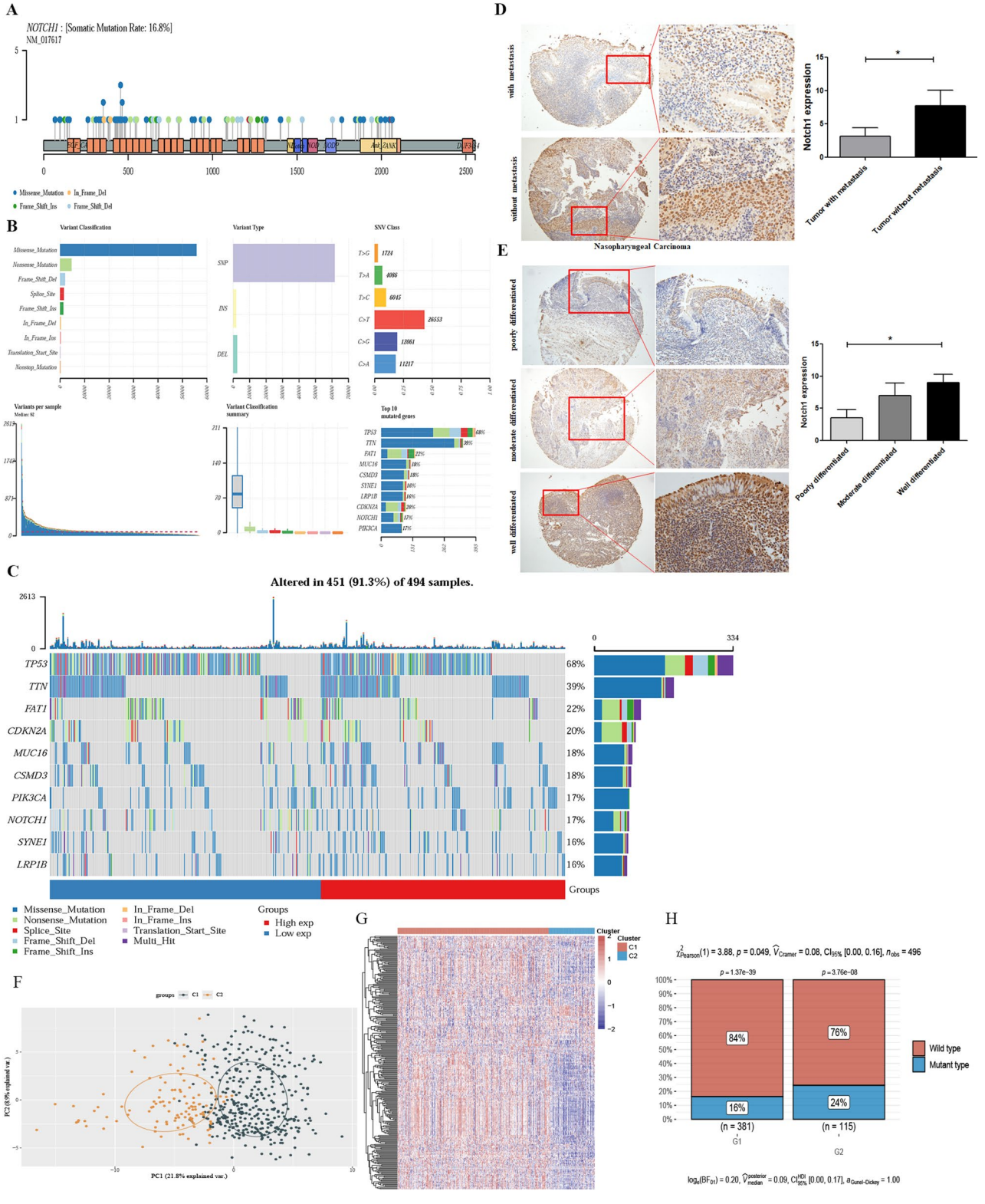

Fig. 1 (See legend on next page.)

(See figure on previous page.)

Fig. 1 Landscape of Notch1 alterations and the relevance to metastasis and EMT in HNSCC. **A** Schematic diagram illustrating the sites and frequencies of NOTCH1 somatic mutations. **B** Summary of somatic mutation characteristics in the HNSCC cohort, including variant classification, variant type, SNV class, variants per sample, and the top ten mutated genes. **C** Oncoplot depicting the mutation landscape of the HNSCC cohort (n = 494), with genes ranked by mutation frequency. The bottom annotation bar indicates the expression groups. **D** Representative immunohistochemical (IHC) images of Notch1 expression in nasopharyngeal carcinoma (NPC) tissues with and without metastasis (Left). The bar chart shows the quantification of Notch1 expression levels (Right). Data are presented as mean ± SD (n = 75; *P < 0.05). **E** Representative IHC images of Notch1 expression in NPC tissues with poor, moderate, and well differentiation (Left). The bar chart displays the quantification of Notch1 expression across differentiation grades (Right) (*P < 0.05). **F** Principal Component Analysis (PCA) plot showing the distribution of the TCGA HNSCC cohort based on consensus clustering of EMT-related gene sets (Groups: C1 and C2). **G** Heatmap visualizing the differential gene expression patterns between the C1 and C2 subtypes. **H** Bar chart comparing the proportions of Notch1 wild-type and mutant samples between the C1 (n = 381) and C2 (n = 115) subgroups. Statistical significance was determined using the Pearson Chi-square test (p = 0.049)

membranes. And then immuno-blotted with primary antibodies at 4 ℃ for overnight. After immunoblotting with secondary antibody (donkey anti-rabbit immunoglobulin G, cat. no. 926–3221) at room temperature for 1 h, the membranes were scanned, and infrared imaging was carried out using the Odyssey CLx Infrared Imaging System (LI-COR, USA).

Transwell Assay

The Matrigel matrix glue (BD Company) was place on ice and melted. According to the ratio of serum-free medium: Matrigel glue = 8:1, the Matrigel working solution was prepared and placed on ice. 80 μl working solution was used to spread glue in the upper chamber of transwell chamber, and then placed at a constant temperature of 37 ℃ for 2 h until Matrigel solidified. After adjusting the cell concentration to 5×10^5/ml, 100 μl was inoculated into the upper chamber, and 600 μl medium containing 20% FBS was added to the lower chamber. After 24 h of culture, excess cells in the upper room were wiped off with a medical cotton swab, and the supraependymal cells 30 min were fixed with 600 μl formaldehyde at room temperature. 0.1% crystal violet staining 10 min, pre-cooling PBS cleaning, drying the lower surface at room temperature, then taking pictures under a positive microscope.

Scratch Assay

Logarithmic growth phase cells were digested and adjusted to a density of 5×10^5 / ml. Each well was inoculated with 1 ml of the cell suspension in a six-well plate. After the cells adhered to the wall and grew fully, they were starved in serum-free medium for 12 h, and the cell surface was marked perpendicular to the orifice plate with 200 μl pipette, resulting in cell scratches. The scratched cells were carefully removed. Images were captured at different times (0, 24 h) under an inverted microscope.

Animal Experiments

32 male nude mice (3–4 weeks old) were purchased from the Vital River Laboratory Animal Technology (Beijing, China) and raised under conditions free of specific pathogens. Animal experiments were approved by the Medical Ethics Committee of Renmin Hospital of Wuhan University. After one week of adaptive feeding, nude mice were randomly and equally distributed to the control and experimental groups. The cells were suspended in serum-free medium at a concentration of 1×10^7/ml. 0.1 ml of cell suspension was subcutaneously injected into the right axilla of each mouse. After 3 weeks, the mice were euthanized and the transplanted tumors were removed.

Statistical Analysis

Statistical analyses were performed using SPSS version 16.0 software. For in vitro and in vivo experiments as well as molecular data analysis, one-way analysis of variance (ANOVA) was used for comparisons among multiple groups, while Student's t-test was used for comparisons between two groups. Categorical data were compared using the chi-square test or Fisher's exact test. Survival analysis was conducted using the Kaplan–Meier method, and survival curves were plotted. A P value < 0.05 was considered statistically significant. For data analysis of the TCGA HNSCC cohort, statistical significance between two groups was assessed by the Wilcoxon rank-sum test, while significance among three or more groups was assessed by the Kruskal–Wallis test.

Results

Expression Characteristics of Notch1 in HNSCC and Its Correlation with Tumor Progression and Immune Microenvironment

To clarify the clinical and biological significance of Notch1 in head and neck squamous cell carcinoma (HNSCC), we first examined its mutational landscape in the TCGA-HNSCC cohort. Analysis of somatic mutation data showed that NOTCH1 was mutated in 16.8% of patients, ranking among the ten most frequently altered genes in HNSCC, with missense mutations and single nucleotide polymorphisms representing the predominant alteration types (Fig. 1A–C). Consensus clustering based on epithelial-mesenchymal transition (EMT)-related genes further stratified the cohort into two molecular subgroups (C1 and C2), which displayed significantly different NOTCH1 mutation frequencies (Fig. 1F–H). These

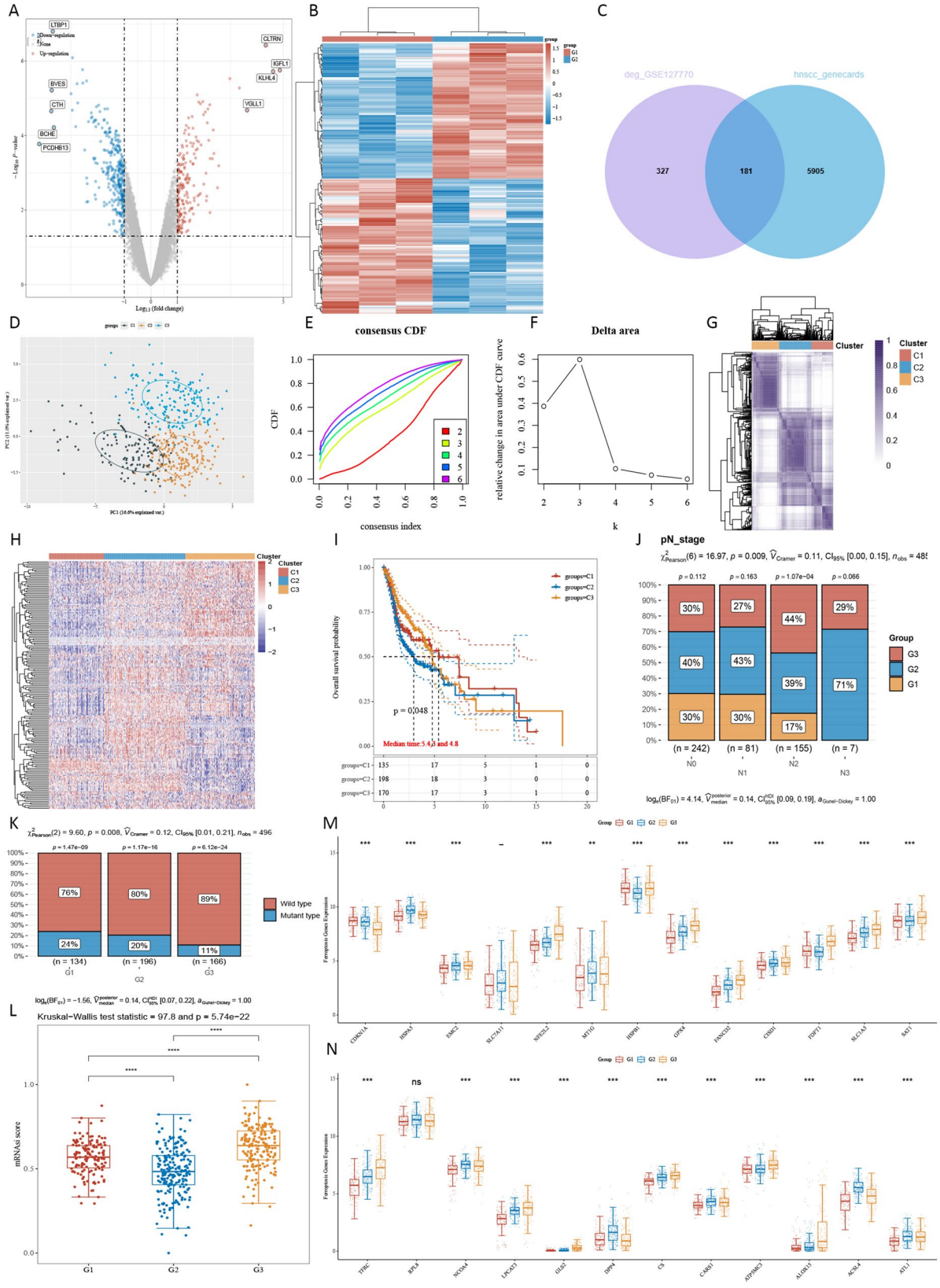

Fig. 2 (See legend on next page.)

(See figure on previous page.)

Fig. 2 Integrated analysis of Notch1 associated gene subtypes and phenotypes in HNSCC. **A** GSE127770 dataset examines gene expression profiles of NOTCH1-truncating mutant OSCC cell line SJG6 before and after restoration of NICD (control vs. NICD group). Volcano plot illustrating differential gene expression between the control and NICD-restored groups. **B** Heatmap visualizing the expression patterns of the differentially expressed genes identified in the GSE127770 dataset.. **C** Venn diagram displaying the intersection of differentially expressed genes from GSE127770 and HNSCC-related genes obtained from GeneCards (Overlap n = 181). **D** Principal Component Analysis (PCA) plot showing the distribution of TCGA HNSCC samples based on the consensus clustering of the 181 overlapping genes. Colors represent the three identified subtypes (C1, C2, and C3). **E** Consensus Cumulative Distribution Function (CDF) plot for cluster numbers k = 2 to 6. **F** Plot of the relative change in area under the CDF curve for k = 2 to 6. **G** Consensus clustering matrix heatmap for k = 3. **H** Heatmap showing the gene expression profiles of the 181 overlapping genes across the three subtypes. **I** Kaplan-Meier curves comparing Overall Survival (OS) among the three subtypes (C1: n = 135, C2: n = 198, C3: n = 170). P-value was calculated using the log-rank test (p = 0.048). **J** Stacked bar chart showing the distribution of pathological N stages (N0–N3) across the three subtypes (n = 485). Statistical significance was assessed using the Pearson Chi-square test (p = 0.009). **K** Bar chart comparing the proportions of Notch1 wild-type and mutant samples among the three subtypes (G1: n = 134, G2: n = 196, G3: n = 166). The P-value indicates significance from the Pearson Chi-square test (p = 0.008). **L** Box plots displaying the mRNAsi scores (stemness index) for the three subtypes. The global P-value was determined by the Kruskal-Wallis test (p = 5.74e-22). ****P < 0.0001. **M**, **N** Box plots showing the expression levels of ferroptosis-related genes across the three subtypes. Statistical significance levels are indicated by asterisks: *P < 0.05, **P < 0.01, ***P < 0.001

findings indicate that NOTCH1 alteration is a common event in HNSCC and may be linked to EMT-associated molecular heterogeneity.

To determine whether aberrant Notch1 expression is associated with metastatic progression in nasopharyngeal carcinoma (NPC), we next evaluated Notch1 protein expression in NPC tissue microarrays by immunohistochemistry. Notch1 expression was markedly decreased in NPC tissues and was significantly associated with tumor differentiation status and lymph node metastasis (N stage) (Figure 1D–E). These results suggest that reduced Notch1 expression is closely related to a more aggressive clinicopathological phenotype and support a potential metastasis-suppressive role for Notch1 in NPC.

To identify downstream transcriptional programs regulated by Notch1, we analyzed the GSE127770 dataset and compared Notch1-deficient cells with cells in which Notch1 signaling was restored (SJG6+NICD). This comparison identified 508 differentially expressed genes (DEGs) associated with Notch1 activity (Figure 2A–B). Intersecting these genes with 6,086 HNSCC-related genes from the GeneCards database yielded a Notch1-related gene set (NRGS) of 181 genes (Figure 2C). Based on the expression pattern of this NRGS, consensus clustering further divided the samples into three subgroups, designated C1, C2, and C3 (Figure 2D–H). These results define a robust Notch1-associated transcriptional signature that captures molecular heterogeneity across HNSCC samples.

To assess the clinical and biological relevance of these Notch1-related subgroups, we performed multidimensional analyses integrating survival, clinicopathological characteristics, stemness, ferroptosis, and immune features. Significant differences were observed among the three subgroups in overall survival (Fig. 2I), N stage (Fig. 2J), NOTCH1 mutation status (Fig. 2K), tumor stemness index (mRNAsi) (Fig. 2L), ferroptosis-related gene expression (Fig. 2M–N), immune cell composition (Figure S2A–D), and immune checkpoint expression (Figure S2E). Among these subgroups, C2 exhibited the highest NOTCH1 mutation frequency and the worst overall survival. These data indicate that the Notch1-related classification is clinically meaningful and identifies a subgroup with particularly aggressive disease behavior.

To further interpret the biological features of the C2 subgroup, we examined differentiation status, stemness, EMT characteristics, and immune contexture. As NOTCH1 is a key regulator of squamous differentiation in HNSCC, and its mutations are predominantly loss-of-function events, disruption of NOTCH1 likely contributes to dedifferentiation. Consistent with this concept, the C2 subgroup displayed a significantly increased mRNAsi score together with a shift toward a mesenchymal phenotype, characterized by reduced epithelial markers and increased mesenchymal markers and EMT-related transcription factors (Figure S1A–E). In addition, C2 showed reduced infiltration of CD8 + T cells, increased proportions of immunosuppressive M2 macrophages, and markedly elevated TIDE scores (Figure S2). These findings suggest that NOTCH1 dysfunction is associated not only with enhanced stem-like and EMT features but also with the establishment of an immunosuppressive, immune-evasive microenvironment, thereby helping to explain the poor prognosis observed in this subgroup.

To explore potential signaling mechanisms downstream of Notch1, we next analyzed the expression of key regulators involved in the PI3K/AKT pathway. Differential expression analysis revealed significant alterations in multiple PI3K/AKT-related molecules, including transcription factors, cell-cycle regulators, and apoptosis- and proliferation-associated proteins, across the three subgroups (Figure S3). These results suggest that Notch1 may interact closely with the PI3K/AKT signaling axis and that this pathway may contribute to Notch1-mediated regulation of EMT and the immune microenvironment.

Overall, our results demonstrate that Notch1 is frequently altered and downregulated in HNSCC/NPC and

that its dysfunction is associated with lymph node metastasis, EMT activation, stemness enhancement, PI3K/AKT pathway dysregulation, and an immunosuppressive tumor microenvironment. Together, these data support a tumor-suppressive role for Notch1 in NPC progression and highlight its potential value as both a prognostic biomarker and a therapeutic target.

Single-cell Transcriptomic Analysis Supports that Notch1 Suppresses Stemness and Metastatic Potential in NPC by Maintaining Epithelial Differentiation

To overcome the limitations of using HNSCC datasets and to more precisely characterize the role of Notch1 in the nasopharyngeal carcinoma (NPC) microenvironment, we analyzed a publicly available single-cell RNA sequencing (scRNA-seq) dataset of NPC patients. Specifically, we obtained the raw scRNA-seq data from the GSE150825 dataset and performed downstream single-cell transcriptomic analysis. UMAP visualization revealed the cellular landscape of NPC, identifying a distinct cluster of epithelial tumor cells together with diverse immune and stromal populations (Fig. 3A).

To rigorously confirm the malignant identity of these epithelial cells, we inferred somatic copy number variations (CNVs) using inferCNV. The analysis revealed extensive genomic instability in the epithelial cluster compared to reference T cells. Specifically, we observed widespread chromosomal alterations across the genome, a hallmark of malignancy, in contrast to the stable genome of immune cells (Fig. 3B). This genomic evidence confirms that the analyzed epithelial cluster consists of bona fide malignant NPC tumor cells, validating the suitability of this dataset for investigating tumor-intrinsic mechanisms.

Having validated the malignant identity of these cells, we next sought to clarify the functional consequence of Notch1 expression within the tumor population. We stratified tumor cells into Notch1-High and Low subpopulations and performed differential expression analysis. As expected, Notch1 was significantly upregulated in the High group. However, classical EMT drivers and mesenchymal markers, such as VIM and FN1, showed no significant upregulation and were retained in the non-significant range (Fig. 3C). This suggests that Notch1 expression is uncoupled from the transcriptional activation of the EMT program in NPC.

To further elucidate the cellular state regulated by Notch1, we applied CytoTRACE to predict the differentiation potential of tumor cells. Surprisingly, NOTCH1-High cells exhibited significantly lower predicted stemness scores (indicating a more differentiated state) compared to the Notch1-Low group (Fig. 3D). Consistently, correlation analysis revealed a significant negative correlation ($R = -0.56, P < 0.001$) between Notch1 expression and the CytoTRACE stemness score (Fig. 3E).

Taken together, these single-cell data provide compelling clinical evidence that Notch1 functions to maintain a differentiated epithelial phenotype in NPC. Its loss (or low expression) is associated with a dedifferentiated, high-stemness state, which is a prerequisite for EMT and metastasis, thereby corroborating our in vitro findings that Notch1 acts as a metastasis suppressor.

CRISPR/Cas9-Mediated Notch1 Knockout in CNE-2 Cells Promotes EMT and Metastasis In Vitro and In Vivo

We tested Notch1 protein expression in six NPC cell lines (CNE2, 5-8F, CNE1, 6-10B, C666-1, and HNE1) (Figure 4A). To define the function of Notch1 in NPC, we generated a CRISPR/Cas9-mediated Notch1 knockout in the NPC cell line CNE-2 and established a stable CNE-2-Notch1-/- cell line (Figure 4B). The expression levels of Notch1 were verified at both the mRNA and protein levels (Figure 4C). Clonogenic growth and CCK-8 assay were carried out, and the results showed that the proliferative capacity increased after Notch1 knockout (Figure 4D-E). The migration ability was significantly increased compared with the control group, and the scratches were healed after 24 hours (Figure 4F-G); The invasive ability in the Notch1-/-group compared with the control group increased significantly (Figure 4G). This evidence structurally confirms that Notch1 knockout may promote the occurrence of invasion and migration of NPC cells. To evaluate the role of Notch1 in vivo, we established a subcutaneous xenograft model in nude mice using CNE-2-Notch1-/- cells (Figure 4H). Cells were injected subcutaneously into the right flank of nude mice, and the animals were maintained under SPF conditions for 4 weeks. Tumor volume was significantly greater in the CNE-2-Notch1-/- group than in the control group. We further evaluated EMT marker expression in xenograft tissues by immunohistochemistry (Figure 4I). Compared with the control group, epithelial marker expression was significantly decreased in the Notch1-/- group, whereas mesenchymal marker expression was significantly increased (Figure 4I).

Subsequently, The cytoskeletal protein F-actin was stained by immunofluorescence staining, and it was found that the cytoskeleton morphology changed after Notch1 knockout, which showed that the cell structure was loose and morphological abnormal (Fig. 5A). EMT markers were detected by western blotting and immunofluorescence respectively (Fig. 5B-C). The expression of epithelial markers expression in the Notch1$^{-/-}$group was significantly decreased compared to that in the control group, while mesenchymal markers expression increased significantly, which was also supported by the immunofluorescence experiment. These results indicated that

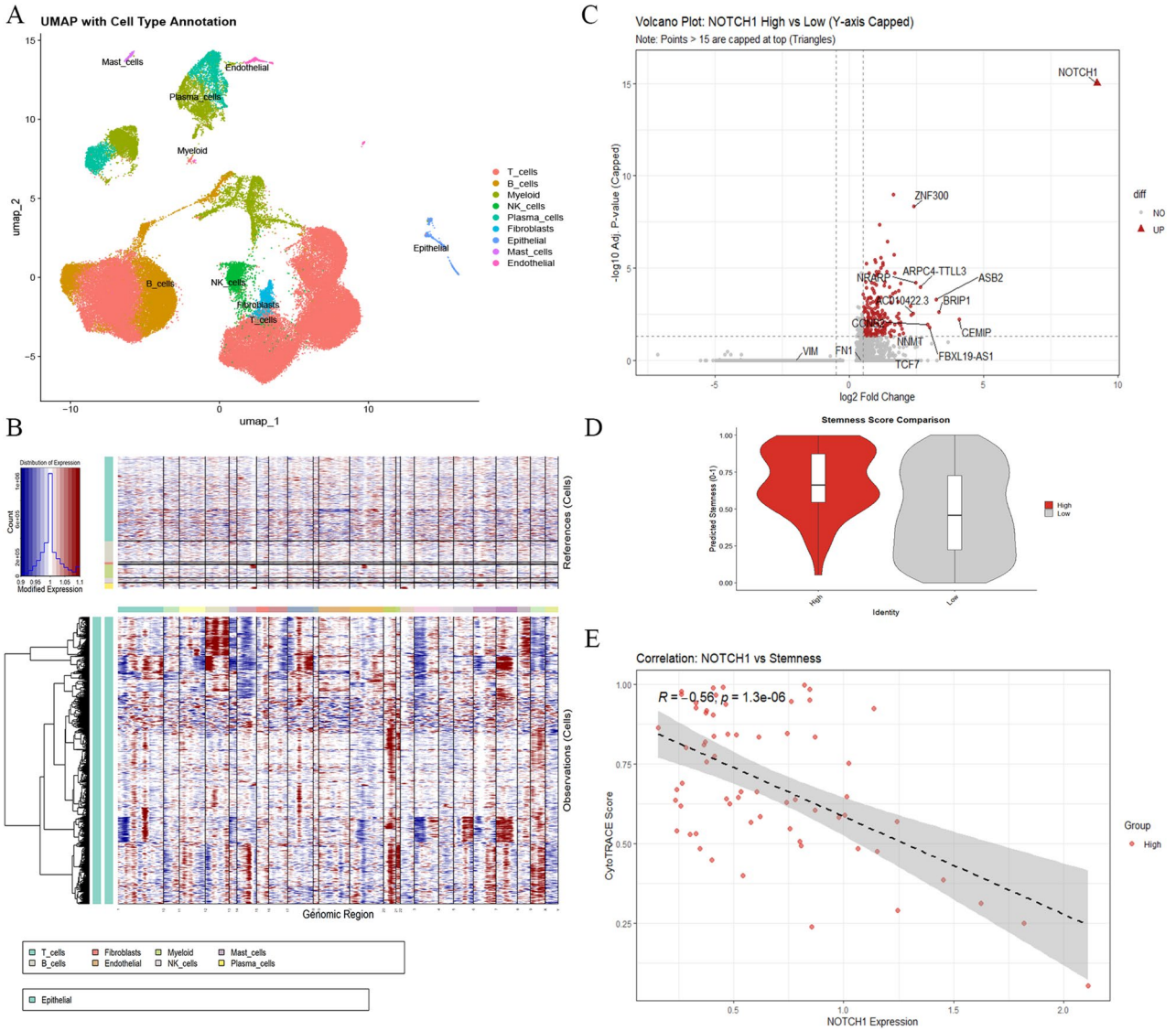

Fig. 3 Single-cell transcriptomic analysis reveals that Notch1 expression is associated with epithelial differentiation and dissociated from EMT in NPC. **A** UMAP projection of the NPC tumor microenvironment, visualizing major cell populations including epithelial tumor cells, T cells, B cells, myeloid cells, and fibroblasts. **B** Inferred CNV heatmap distinguishing malignant epithelial cells (Observations, bottom) from reference T cells (References, top). The extensive genomic instability (red/blue patterns reflecting chromosomal amplifications and deletions) across the genome confirms the malignant identity of the identified epithelial cluster. **C** Volcano plot of differentially expressed genes (DEGs) between Notch1-High and Notch1-Low tumor cells. While Notch1 is significantly upregulated (red triangle), classical EMT markers such as VIM and FN1 show no significant upregulation (grey area), indicating that Notch1 expression does not drive the EMT program. **D** Violin plot comparing CytoTRACE differentiation scores. Notch1-High cells exhibit significantly lower stemness scores compared to the Notch1-Low group (P<0.001P<0.001), suggesting that Notch1 functions to maintain a differentiated epithelial state. **E** Scatter plot showing a significant negative correlation (R=−0.56) between Notch1 expression and the predicted stemness score, further supporting the role of Notch1 in suppressing dedifferentiation-associated plasticity

Notch1 significantly inhibited the invasive ability of NPC cells through the inhibition of EMT.

Based on these results, it could be speculated that Notch1 knockout induced NPC EMT in vivo and in vitro.

Lentiviral Notch1 Overexpression in CNE-2 Cells Inhibits EMT and Tumor Invasion In Vitro and In Vivo

To further confirm the functional impact of Notch1 overexpression on the invasiveness of NPC cells, we used a lentiviral vector to generate a stable Notch1-overexpressing CNE-2 cell line (CNE-2-lvNICD1) (Fig. 5D) The invasive ability and EMT markers were detected by transwell and western blot assays, respectively. The number of cells passing through the membrane was significantly decreased compared with that in the control group in both the invasion and migration assay (Fig. 5E). Meanwhile, the expression of EMT epithelial molecular markers E-cadherin and ZO-1 were higher than that

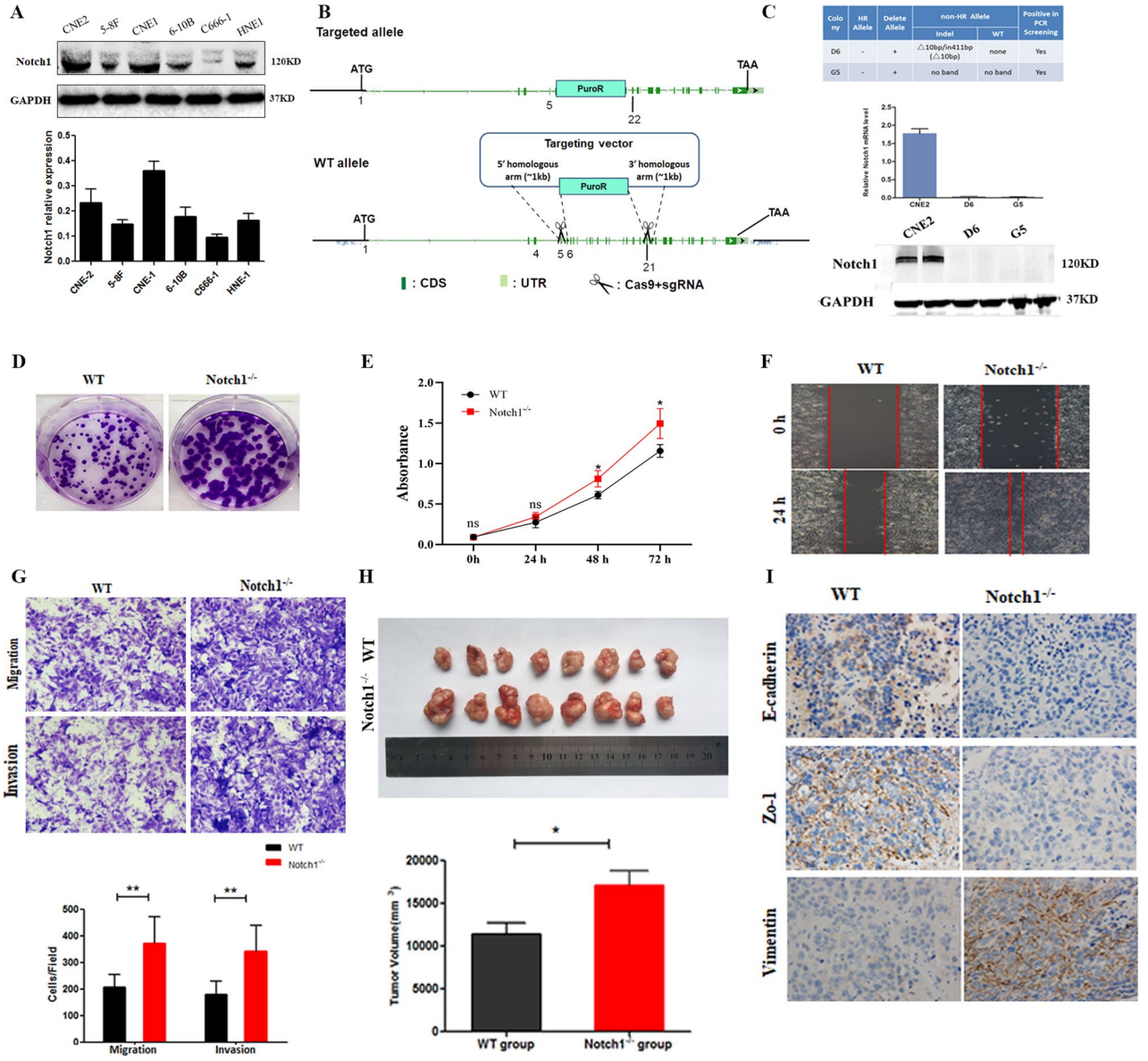

Fig. 4 CRISPR/Cas9-mediated Notch1 knockout in CNE-2 cells promotes EMT and metastasis in vitro and in vivo **A** Western blot analysis of Notch1 protein expression in six NPC cell lines (CNE2, 5-8F, CNE1, 6-10B, C666-1, and HNE1). **B** Schematic diagram of the CRISPR/Cas9 gene-editing strategy, illustrating the wild-type (WT) allele and the targeted allele with the PuroR cassette insertion. **C** Verification of Notch1 knockout efficiency. Top: Table summarizing the indel mutations in clones D6 and G5. Middle: RT-qPCR analysis of Notch1 mRNA levels in WT and knockout clones. Bottom: Western blot confirming the absence of Notch1 protein in D6 and G5 clones. **D** Representative images of colony formation assays for WT and Notch1-/- CNE-2 cells. **E** Cell proliferation curves determined by CCK-8 assay at 0, 24, 48, and 72 hours. **F** Representative images of the wound healing scratch assay at 0 h and 24 h. **G** Transwell migration and invasion assays. Top: Representative micrographs of migrated and invaded cells stained with crystal violet. Bottom: Bar charts showing the quantification of cell numbers per field. (**P < 0.01). **H** In vivo tumorigenesis and metastasis analysis. Top: Macroscopic photographs of subcutaneous tumors excised from the WT and Notch1-/- groups (n = 8 mice per group). Bottom: Bar chart comparing the tumor volumes (*P < 0.05). **I** Representative immunohistochemical (IHC) staining images of EMT-related markers (E-cadherin, ZO-1, and Vimentin) in the excised tumor xenograft tissues from WT and Notch1-/- groups

in the control group, while the expression of mesenchymal marker vimentin were lower (Fig. 5F). Similar results were obtained for immunofluorescence detection (Fig. 5G). These results further demonstrated that Notch1 played a tumor suppressor role in NPC and may inhibit NPC metastasis by inhibiting the EMT phenotype.

To evaluate the role of Notch1 in vivo, we established a subcutaneous xenograft model in nude mice using CNE-2-lvNICD1 cells. The size of the primary tumors were evaluated. The results showed that the volume of the transplanted tumors was significantly smaller in

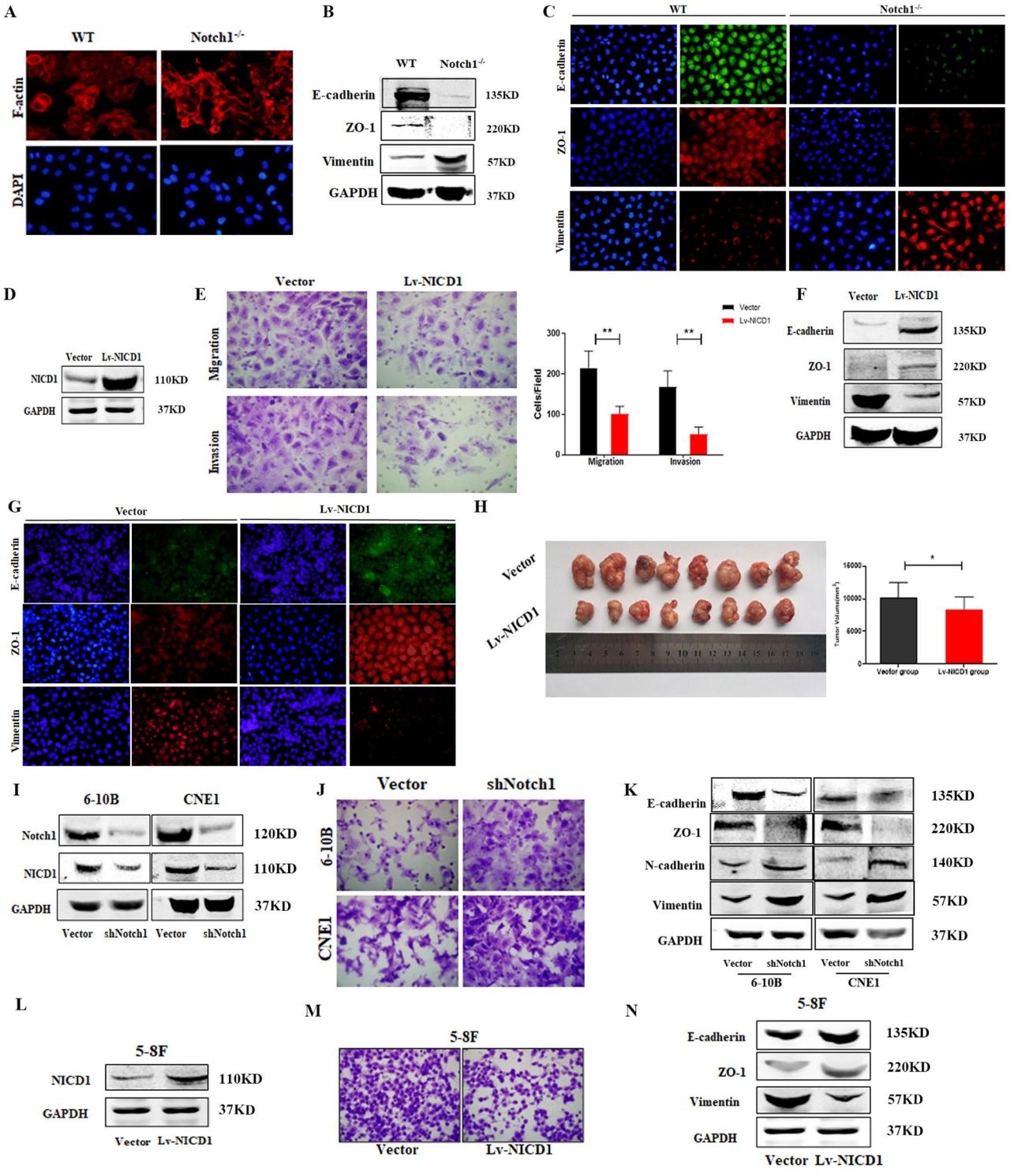

Fig. 5 (See legend on next page.)

the CNE-2-lvNICD1 group than in the control group (Fig. 5H).

Validation of the EMT-Suppressive Role of Notch1 Across NPC Cell Lines with Distinct Metastatic Potential

To determine whether the EMT-suppressive effect of Notch1 is generalizable across NPC, we included three other NPC cell lines with different invasion and

(See figure on previous page.)

Fig. 5 Notch1 regulates EMT and metastasis in NPC cell lines in vitro and in vivo **A** Representative immunofluorescence images showing F-actin (red) cytoskeletal staining and DAPI (blue) nuclear counterstaining in wild-type (WT) and Notch1-/- CNE-2 cells. **B** Western blot analysis of epithelial (E-cadherin, ZO-1) and mesenchymal (Vimentin) markers in WT and Notch1-/- CNE-2 cells. GAPDH was used as a loading control. **C** Representative immunofluorescence staining of E-cadherin (green), ZO-1 (red), and Vimentin (red/blue) in WT and Notch1-/- CNE-2 cells. **D** Western blot analysis confirming the overexpression efficiency of Notch1 in CNE-2 cells transduced with the empty vector or lentiviral NICD (Notch1 intracellular domain). **E** Transwell migration and invasion assays for Vector and NICD CNE-2 cells. Left: Representative images of migrated and invaded cells. Right: Bar charts showing the quantification of cell numbers per field. (**P < 0.01). **F** Western blot analysis of EMT-related markers (E-cadherin, ZO-1, Vimentin) in Vector and NICD CNE-2 cells. **G** Representative immunofluorescence staining of E-cadherin (green), ZO-1 (red), and Vimentin (red) in Vector and NICD CNE-2 cells. **H** In vivo tumorigenesis assay. Left: Macroscopic images of xenograft tumors excised from the Vector and Lv-NICD1 groups (n = 8 mice per group). Right: Tumor growth curves showing volume changes over time. (*P < 0.05). **I** Western blot analysis of Notch1 and NICD1 protein expression in 6-10B and CNE1 cells transduced with empty vector or shNotch1. **J** Representative images of Transwell invasion assays for 6-10B and CNE1 cells in the Vector and shNotch1 groups. **K** Western blot analysis of EMT markers (E-cadherin, ZO-1, N-cadherin, and Vimentin) in 6-10B and CNE1 cells upon Notch1 knockdown. **L** Western blot validation of NICD1 overexpression in 5-8F cells transduced with empty vector or Lv-NICD1. **M** Representative images of Transwell invasion assays for 5-8F cells in the Vector and Lv-NICD1 groups. **N** Western blot analysis of EMT markers (E-cadherin, ZO-1, and Vimentin) in 5-8F cells upon Notch1 overexpression

metastasis capabilities (5–8 F, CNE-1, and 6-10B). Based on their different metastatic abilities, we constructed 5–8 F-lvNICD1, CNE-1-shNotch1, and 6-10B-shNotch1 (Fig. 5I, L). We then detected the changes in invasiveness after Notch1 knockdown and overexpression, as well as the changes in EMT markers. Compared with the control group, the number of cells passing through the membrane increased significantly in the Notch1 knockdown group (Fig. 5J). In the western blot assay, E-cadherin and ZO-1 expression decreased significantly, while vimentin expression was significantly increased in the Notch1 knockdown group (Fig. 5K). In the control group, the transwell assay showed that the number of cells passing through the membrane was lower in both Notch1 overexpression group (Fig. 5M). In the western blot assay, E-cadherin and ZO-1 showed higher expression, while vimentin expression were lower compared with the Notch1 overexpression group (Fig. 5N). These results were consistent with the previous results. Notch1 was negatively correlated with the occurrence of NPC EMT, and was suspected to play a role as a tumor suppressor in NPC metastasis. These results, together with the CNE-2 gain- and loss-of-function models, indicate that Notch1 consistently suppresses EMT and invasive behavior across NPC cell lines with distinct metastatic potential.

Notch1 Regulates Smad3 Phosphorylation and Nuclear Translocation in NPC Cells

Following the phenotypic and preliminary mechanistic explorations, we further explored the downstream molecular mechanism of Notch1. We performed Western blot analysis to detect downstream molecules in Notch1 knockout cells compared to the control group (Fig. 6A), and found that P-Smad3 showed a significant difference, suggesting a close relationship with Notch1. Consequently, we performed correlation analysis between the two using TCGA data. TCGA data analysis additionally showed a significant positive correlation between Notch1 and SMAD3 expression (Fig. 6B).

To further investigate the tumor-suppressive role of Notch1 in NPC, we further analyzed the molecular mechanism of Notch1 and its downstream Smad3 interaction. Our results demonstrated that following Notch1 knockout in CNE-2 cells, total Smad3 expression remained unchanged while p-Smad3 levels increased. Further subcellular fractionation revealed that Notch1 depletion led to a reduction of total Smad3 in the cytoplasm and a concurrent accumulation of total Smad3 in the nucleus (Fig. 6C). Immunofluorescence also confirmed that p-Smad3 was predominantly localized in the nucleus of Notch1-deficient cells (Fig. 6D).

To validate these findings, we treated cells with a specific Smad3 inhibitor (SIS3). EMT marker detection indicated that Notch1 knockout increased the expression of E-cadherin and ZO-1 while decreasing vimentin expression, and these changes were reversed upon SIS3 treatment (Fig. 6E).Transwell assays showed that Notch1 knockout enhanced cell invasion, whereas SIS3 treatment reduced this invasive ability to nearly control levels (Fig. 6F).

Conversely, in Notch1-overexpressing CNE-2-lvNICD1 cells, p-Smad3 levels were significantly decreased while total Smad3 remained unaffected. Subsequent nuclear and cytoplasmic extraction further demonstrated that Notch1 overexpression resulted in an accumulation of total Smad3 in the cytoplasm and a corresponding decrease in the nucleus (Fig. 6H), a result further supported by immunofluorescence staining (Fig. 6I). Upon treatment of these cells with the Smad3 activator TGFβ1, invasion abilities were enhanced (Fig. 6G), accompanied by downregulation of E-cadherin and ZO-1 and upregulation of vimentin (Fig. 6J) Taken together, these results demonstrate that Notch1 regulates EMT in NPC cells by modulating the phosphorylation and nuclear translocation of Smad3, thereby affecting the metastatic and invasive capabilities of NPC cells.

Notch1 Regulates Smad3 Phosphorylation and Modulates Smad3/AKT Interaction

Previous studies have reported that AKT can interact with the non-activated form of Smad3. We hypothesized that upon Notch1 knockout, Smad3 dissociates

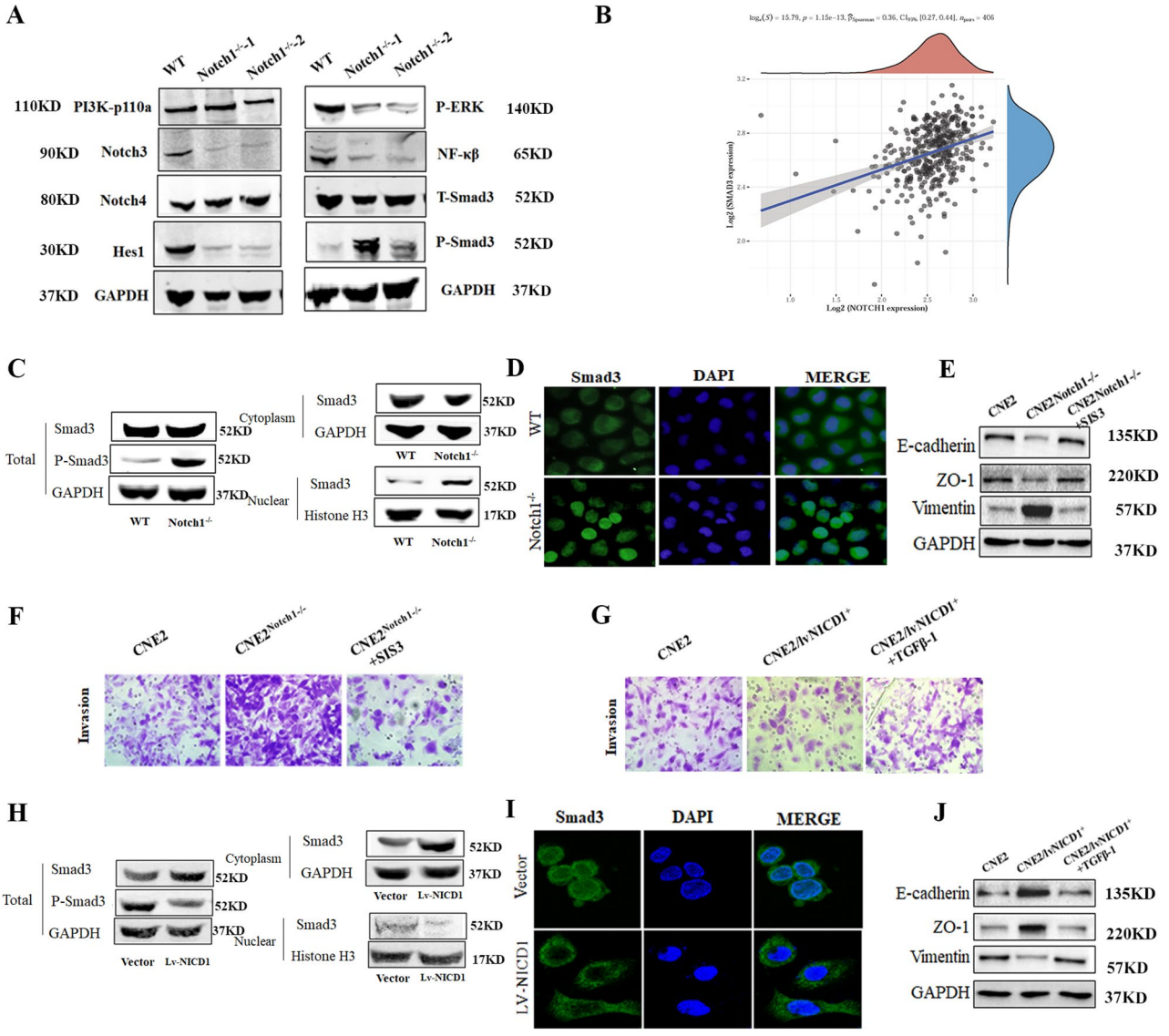

Fig. 6 Notch1 regulates Smad3 phosphorylation and nuclear translocation in CNE2 cells. **A** Western blot analysis of downstream signaling molecules (PI3K-p110α, Notch3, Notch4, Hes1, P-ERK, NF-κB, Total-Smad3, and P-Smad3) in wild-type (WT) and Notch1-/- CNE-2 cells. GAPDH was used as a loading control. **B** Scatter plot with marginal density diagrams displaying the correlation between NOTCH1 and SMAD3 mRNA expression levels. The Spearman correlation coefficient (ρ=0.36), P-value (p=1.15×10e−13), and sample size (n=405) are indicated. **C** Western blot analysis of total and phosphorylated Smad3 levels (Left) and subcellular fractionation of Smad3 (Right) in WT and Notch1-/- cells. Histone H3 and GAPDH were used as nuclear and cytoplasmic loading controls, respectively . **D** Representative immunofluorescence images of Smad3 (green) and DAPI (blue) in WT and Notch1-/- cells. **E** Western blot analysis of EMT markers (E-cadherin, ZO-1, Vimentin) in CNE-2, Notch1-/-, and Notch1-/- cells treated with the Smad3 inhibitor SIS3. **F** Representative images of Transwell invasion assays for CNE-2, Notch1-/-, and Notch1-/- + SIS3 cells. **G** Representative images of Transwell invasion assays for CNE-2, CNE-2-lvNICD1, and CNE-2-lvNICD1 cells treated with TGF-β1. **H** Western blot analysis of total and phosphorylated Smad3 levels (Left) and subcellular fractionation of Smad3 (Right) in Vector and Lv-NICD1 cells. **I** Representative immunofluorescence images of Smad3 (green) and DAPI (blue) in Vector and Lv-NICD1 cells. **J** Western blot analysis of EMT markers (E-cadherin, ZO-1, Vimentin) in CNE-2, CNE-2-lvNICD1, and CNE-2-lvNICD1 cells treated with TGF-β1

from AKT, becomes phosphorylated and activated, and then translocates into the nucleus to promote the EMT process. To test this hypothesis, CNE-2-Notch1-/- cells were treated with the AKT agonist insulin and the Smad3 inhibitor SIS3. The results showed that P-Smad3 expression was significantly increased in Notch1 knockout cells, decreased following SIS3 treatment, and elevated again upon subsequent addition of insulin (Fig. 7A). Similarly, Transwell assays demonstrated that Notch1 knockout promoted cell invasion and migration, which were reduced after SIS3 treatment and then enhanced again with insulin supplementation (Fig. 7B). The changes in EMT-related markers followed the same trend: E-cadherin and ZO-1 were downregulated and vimentin was upregulated after Notch1 knockout, while SIS3 treatment upregulated E-cadherin and ZO-1 and downregulated

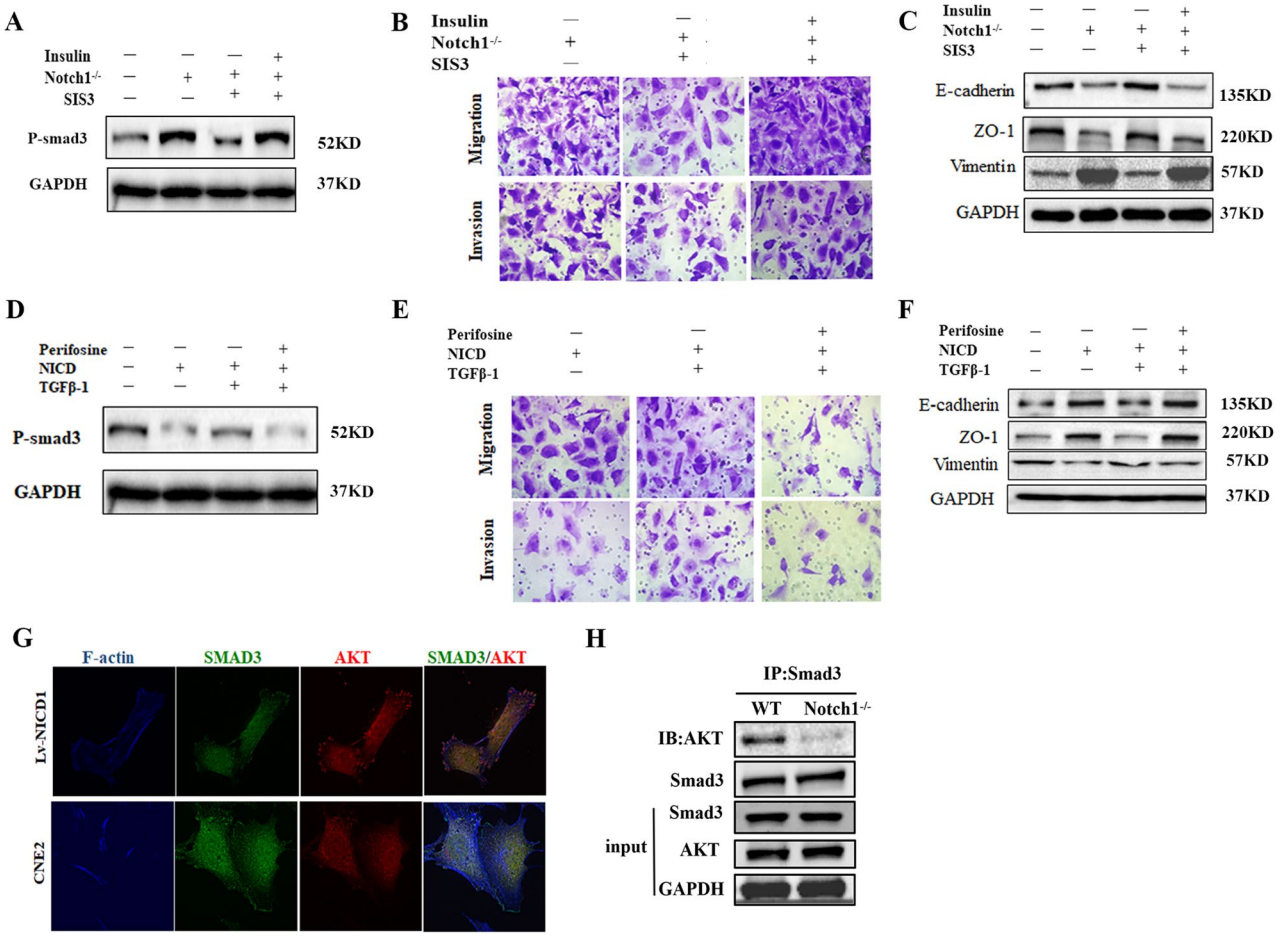

Fig. 7 Notch1 modulates phosphorylation of Smad3 via Smad3/AKT interaction **A** Western blot analysis of P-Smad3, Total-Smad3, P-AKT, and Total-AKT levels in CNE-2-Notch1-/- cells treated with the AKT agonist Insulin or the Smad3 inhibitor SIS3. **B** Representative images of Transwell migration and invasion assays for CNE-2-Notch1-/- cells following treatment with Insulin or SIS3. **C** Western blot analysis of EMT-related markers (E-cadherin, ZO-1, and Vimentin) in CNE-2-Notch1-/- cells treated with Insulin or SIS3. **D** Western blot analysis of P-Smad3, Total-Smad3, P-AKT, and Total-AKT levels in CNE-2-lvNICD1 (Notch1 overexpression) cells treated with the AKT inhibitor Perifosine or TGF-β1. **E** Representative images of Transwell migration and invasion assays for CNE-2-lvNICD1 cells treated with Perifosine or TGF-β1. **F** Western blot analysis of EMT-related markers (E-cadherin, ZO-1, and Vimentin) in CNE-2-lvNICD1 cells treated with Perifosine or TGF-β1. **G** Representative immunofluorescence images showing the localization of AKT (red) and Smad3 (green) in Vector and Lv-NICD1 cells. Nuclei were counterstained with DAPI (blue). **H** Co-immunoprecipitation (Co-IP) assay detecting the protein interaction between AKT and Smad3 in wild-type (WT) and Notch1-/- CNE-2 cells

vimentin; insulin once again promoted EMT marker changes (Fig. 7C).

Moreover, in Notch1-overexpressing CNE-2-lvNICD1 cells, treatment with the AKT inhibitor Perifosine and the Smad3 agonist TGFβ1 produced consistent results in the opposite direction: Notch1 overexpression reduced P-Smad3 expression, which was increased by TGFβ1 and decreased again by Perifosine. The effects on cell invasion, migration, and EMT molecular markers were also opposite to those observed in the knockout group (Fig. 7D-F).

Co-immunoprecipitation assays showed that Smad3 binding to AKT was markedly reduced after Notch1 knockout, and immunofluorescence confirmed their co-localization in cells (Fig. 7G-H). Collectively, these results suggest that Notch1 regulates the interaction between Smad3 and AKT, thereby modulating Smad3 phosphorylation and the EMT process.

Discussion

Notch1 exhibits a high mutation rate in head and neck cancers and is widely recognized as a tumor suppressor gene [3, 11]. Our study confirms that Notch1 functions as a tumor suppressor in NPC and significantly impacts tumor invasion and metastasis. Using genetic knockout in cell lines, xenograft animal models, and clinical tissue microarrays, we demonstrated that decreased Notch1 expression is closely associated with more aggressive phenotypes in NPC, particularly by enhancing tumor metastatic potential.

One of the core mechanisms of cancer metastasis is epithelial–mesenchymal transition (EMT) [6–8]. This

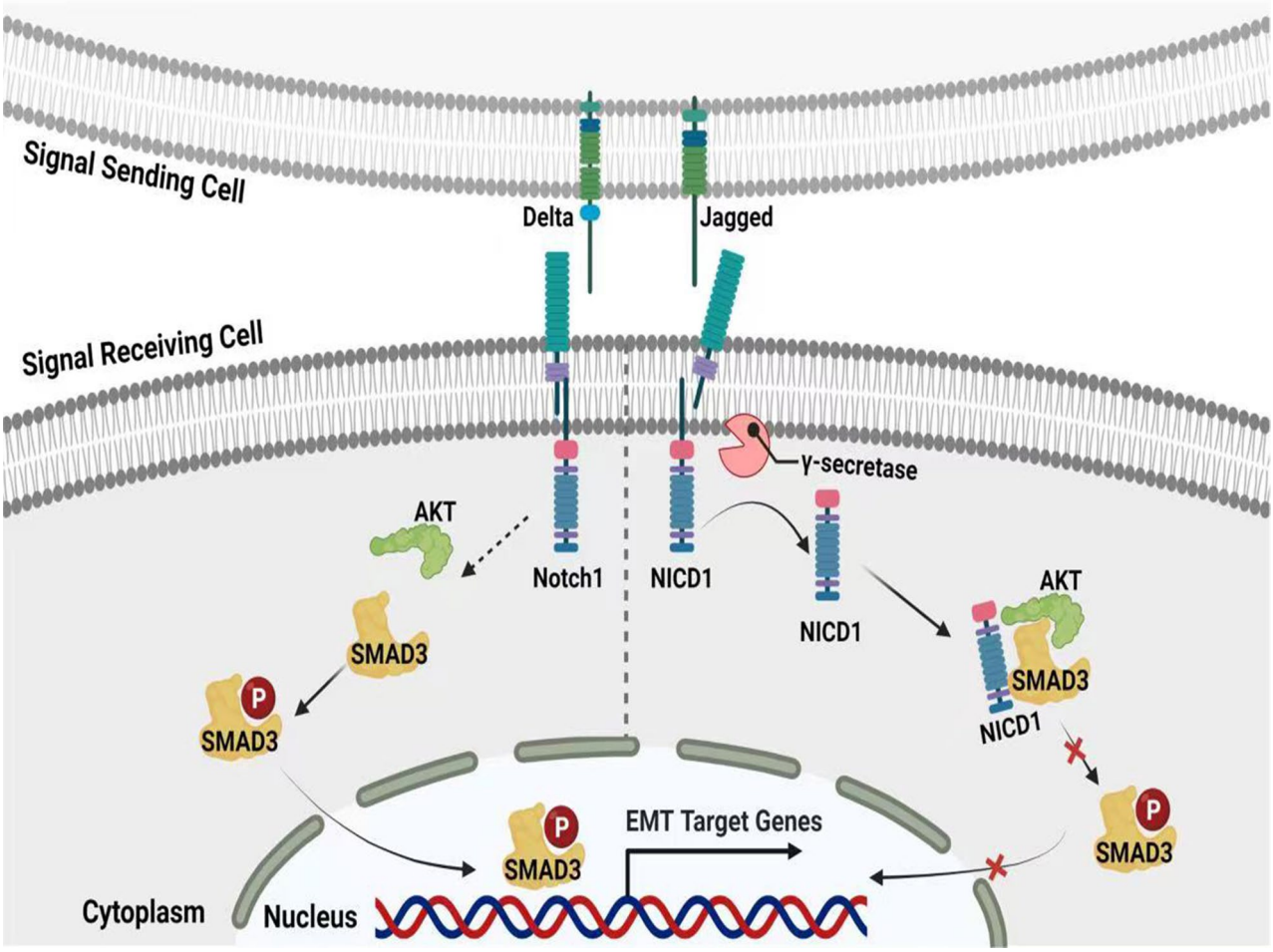

Fig. 8 Schematic illustration of the proposed Notch1-Smad3/AKT axis in NPC. Notch1 binds to the Smad3/AKT complex in the cytoplasm, stabilizing it and preventing Smad3 nuclear entry and EMT activation. Notch1 knockout leads to complex dissociation, Smad3 phosphorylation, nuclear translocation, and EMT induction

study systematically verified that Notch1 negatively regulates the EMT phenotype in NPC cells: Notch1 knockout markedly promoted cell proliferation, migration, and invasion, as well as expression changes in EMT-related markers, while Notch1 overexpression inhibited these malignant characteristics. In vivo models further validated the pivotal role of Notch1 in regulating NPC metastasis.

Although the tumor-suppressive function of Notch1 has been reported by several studies, its precise mechanisms remain incompletely understood. Existing literature suggests that loss of Notch1 may trigger the activation of other pathways such as Wnt and Hedgehog [9, 12, 13]. In addition, there is potential crosstalk between the Notch pathway and immune evasion [14–16]. In our study, we found that Notch1 knockout significantly affects the phosphorylation status of Smad3. Further molecular docking analysis indicated that Notch1 can form a stable complex with Smad3, and the loss of Notch1 leads to increased Smad3 phosphorylation and nuclear translocation, suggesting that Notch1 might suppress Smad3 activation by directly binding to it.

Combining previous studies, which show that Akt binds to the non-activated form of Smad3 [13, 17, 18], we hypothesized that Notch1 maintains the interaction between Smad3 and Akt in NPC cells. Loss of Notch1 disrupts this interaction, causing Smad3 to dissociate from Akt, become phosphorylated and activated, and translocate into the nucleus, thereby inducing EMT and promoting metastasis. Co-IP experiments and molecular docking provided further evidence that after Notch1 knockout, the association between Smad3 and Akt is substantially reduced, supporting this hypothesis.

Based on the results of this study, we propose a molecular mechanism model for Notch1 as a tumor suppressor in NPC (Fig. 8J): Notch1 binds to non-activated Smad3, maintaining its association with Akt and suppressing Smad3 phosphorylation and nuclear translocation. Loss of Notch1 disrupts this suppression, releasing activated Smad3 to drive the EMT process and thus promote

tumor invasion and metastasis. This mechanism offers a novel perspective and molecular basis for understanding Notch1's role in the malignant progression of NPC.

Although significant progress has been made in the study of the Notch signaling pathway, there are currently no FDA-approved targeted therapies for this pathway. The future development of Notch-related biomarkers and rational combination treatment strategies remains a critical research direction. Our study deeply elucidates the mechanism by which Notch1 influences Smad3 phosphorylation, providing a theoretical basis for precision targeting of Notch in therapy.

However, this study has certain limitations, as most experiments were based on cell lines and subcutaneous xenograft models, lacking validation in more clinically relevant metastasis models. Furthermore, the complexity of the tumor microenvironment and the complete Notch1-associated signaling network warrant further investigation. The heterogeneity of Notch1 across different tissues and patient populations also requires validation in larger cohorts.

Notably, in our molecular subtyping analysis based on clustering of 181 candidate genes, the C2 subgroup showed significantly worse survival outcomes and notable upregulation of EMT-related genes. Meanwhile, the C2 group displayed typical features of an immunosuppressive microenvironment: the lowest CD8 + T cell infiltration, the highest abundance of immunosuppressive M2 macrophages, and elevated TIDE scores, indicating enhanced immune evasion. Increasing evidence shows that tumor subtypes with active EMT features often coexist with immunosuppressive environments, mutually promoting each other and collectively facilitating tumor metastasis and therapeutic resistance. EMT not only enhances cellular migratory and invasive capacities but may also promote immune escape by upregulating immune checkpoint molecules and reducing antigen presentation, forming a "cold tumor" state and posing challenges for immunotherapy in the clinic.

Further analysis revealed that despite showing enhanced EMT activity and immune suppression, the C2 subgroup had the lowest mRNAsi score. This indicates a substantial heterogeneity in the mechanisms of malignant progression among molecular subtypes of NPC. For the C2 subtype, malignant progression may be more dependent on EMT activation and immune remodeling rather than classical stemness properties, consistent with some reports that EMT-dominated subtypes score lower for stemness. The mRNAsi score is mainly based on embryonic stem cell expression features and may not fully represent all mechanisms driving malignant progression. These results reflect the complexity and diversity of molecular subtypes and biological behaviors in NPC.

In summary, this study not only confirms the tumor-suppressive role of Notch1 in NPC but also elucidates its mechanism in regulating EMT and the immune microenvironment via the Smad3/Akt axis, providing novel insights for understanding NPC metastasis and guiding therapeutic strategies.

Supplementary Information

The online version contains supplementary material available at https://doi.org/10.1186/s12575-026-00341-5.

Supplementary Material 1: Comparison of EMT-related gene expression across three HNSCC subtypes defined by 181 Notch1-associated genes. Panels (A–E) show the expression differences of genes related to five EMT aspects: (A) epithelial markers, (B) mesenchymal markers, (C) core transcription factors, (D) signaling pathways, and (E) other EMT markers. Statistical significance was assessed using the Kruskal-Wallis test.

Supplementary Material 2: Immune microenvironment analysis of HNSCC subtypes defined by Notch1 associated genes(A, B) Distribution of immune scores among the three subtypes. (C) Immunotherapy response prediction in the three subtypes, with boxplots and scatterplots showing immune response scores. (D) Heatmap of immune cell scores across the three subtypes. (E) Expression differences of immune checkpoint genes among the three subtypes.

Supplementary Material 3: Expression analysis of PI3K/AKT pathway downstream genes across three HNSCC subtypes defined by 181 Notch1-associated genes.(A) Signaling/regulator genes, (B) transcription factors, and (C) cell cycle/apoptosis-related genes are compared among subtypes. Statistical significance was assessed using the Kruskal-Wallis test.

Acknowledgments

Not applicable.

Authors' Contributions

Jingjing Zuo and Mengyuan Dai designed the study. The bioinformatics data in this manuscript were analyzed by Jingjing Zuo. Shiyong Huang and Mengyuan Dai conducted the majority of the experiments. Fen Li and Lei Wang performed animal experiments. Ting Huang and Lei Wang were responsible for collecting clinical samples. Jingjing Zuo, Mengyuan Dai and Chenglin Qi analyzed the data. Jingjing Zuo wrote and Shiyong Huang edited the manuscript. Linfeng Ye and Zezhang Tao were responsible for the overall planning, supervision, improvement, and funding support of the entire experiment. All authors have read and agreed to the contents of the manuscript and have consented to its publication.

Funding

This study was supported by grants from the National Natural Science Foundation of China (no. 82302917), and the Guidance fund of the Renmin Hospital of Wuhan.
University (No. RMYD2018Z12).

Data Availability

All datasets can be accessed using the accession numbers provided in the manuscript.

Declarations

Ethics Approval and Consent to Participate

This study was reviewed and approved by the Ethical Board at Renmin Hospital of Wuhan University.

Consent for Publication

Not applicable.

Competing Interests

The authors declare no competing interests.

Author details
[1]Department of Otorhinolaryngology-Head and Neck Surgery, Renmin Hospital of Wuhan University, 238 Jie Fang Road,, Wuhan, Hubei 430060, P.R. China
[2]Department of Gynecology, Zhongnan Hospital of Wuhan University, Wuhan, Hubei 430060, P.R. China
[3]Institute of Otorhinolaryngology-Head and Neck Surgery, Renmin Hospital of Wuhan University, Wuhan 430060, Hubei, P.R. China
[4]Department of Otorhinolaryngology-Head and Neck Surgery, Zhongnan Hospital of Wuhan University, Wuhan, Hubei 430060, P.R. China
[5]Department of Otolaryngology, The First Affiliated Hospital, Zhejiang University School of Medicine, 79 Qingchun Road, Hangzhou, Zhejiang 310003, P.R. China

Received: 26 January 2026 / Accepted: 24 April 2026
Published online: 29 April 2026

References

1. Juarez-Vignon Whaley JJ, Afkhami M, Onyshchenko M, Massarelli E, Sampath S, Amini A et al. Recurrent/Metastatic Nasopharyngeal Carcinoma Treatment from Present to Future: Where Are We and Where Are We Heading? Current treatment options in oncology. 2023;24(9):1138–66. Epub 2023/06/15. https://doi.org/10.1007/s11864-023-01101-3
2. Chien IA, Hsu YC, Tsai CH, Cheng SP. Population-Based Analysis of the Human Development Index and Risk Factors for Head and Neck Cancer. Head Neck. 2024;46(4):889–95. https://doi.org/10.1002/hed.27639. Epub 2024/01/12.
3. Agrawal N, Frederick MJ, Pickering CR, Bettegowda C, Chang K, Li RJ, et al. Exome Sequencing of Head and Neck Squamous Cell Carcinoma Reveals Inactivating Mutations in NOTCH1. Science. 2011;333(6046):1154–7. https://doi.org/10.1126/science.1206923.
4. Moore G, Annett S, McClements L, Robson T. Top Notch Targeting Strategies in Cancer: A Detailed Overview of Recent Insights and Current Perspectives. Cells. 2020;9(6). https://doi.org/10.3390/cells9061503.
5. Mouillesseaux KP, Wiley DS, Saunders LM, Wylie LA, Kushner EJ, Chong DC, et al. Notch Regulates BMP Responsiveness and Lateral Branching in Vessel Networks via SMAD6. Nat Commun. 2016;7:13247. https://doi.org/10.1038/ncomms13247.
6. Brabletz S, Schuhwerk H, Brabletz T, Stemmler MP. Dynamic EMT: A Multi-Tool for Tumor Progression. EMBO J. 2021;40(18):e108647. https://doi.org/10.15252/embj.2021108647.
7. Dongre A, Weinberg RA. New Insights into the Mechanisms of Epithelial-Mesenchymal Transition and Implications for Cancer. Nat Rev Mol Cell Biol. 2019;20(2):69–84. https://doi.org/10.1038/s41580-018-0080-4.
8. Mullins RDZ, Pal A, Barrett TF, Heft Neal ME, Puram SV. Epithelial-Mesenchymal Plasticity in Tumor Immune Evasion. Cancer Res. 2022;82(13):2329–43. https://doi.org/10.1158/0008-5472.Can-21-4370. Epub 2022/04/02.
9. Pelullo M, Zema S, Nardozza F, Checquolo S, Screpanti I, Bellavia D, Wnt. Notch, and TGF-β Pathways Impinge on Hedgehog Signaling Complexity: An Open Window on Cancer. Front Genet. 2019;10:711. https://doi.org/10.3389/fgene.2019.00711. Epub 2019/09/26.
10. Kar R, Jha NK, Jha SK, Sharma A, Dholpuria S, Asthana N, et al. A NOTCH Deeper into the Epithelial-To-Mesenchymal Transition (EMT) Program in Breast Cancer. Genes. 2019;10(12). https://doi.org/10.3390/genes10120961. Epub 2019/11/27.
11. Shah PA, Huang C, Li Q, Kazi SA, Byers LA, Wang J, et al. NOTCH1 Signaling in Head and Neck Squamous Cell Carcinoma. Cells. 2020;9(12). https://doi.org/10.3390/cells9122677.
12. Blokzijl A, Dahlqvist C, Reissmann E, Falk A, Moliner A, Lendahl U, et al. Cross-talk Between the Notch and TGF-beta Signaling Pathways Mediated by Interaction of the Notch Intracellular Domain with Smad3. J Cell Biol. 2003;163(4):723–8. https://doi.org/10.1083/jcb.200305112.
13. Dong Y, Lakhia R, Thomas SS, Dong Y, Wang XH, Silva KA, et al. Interactions between p-Akt and Smad3 in Injured Muscles Initiate Myogenesis or Fibrogenesis. Am J Physiol Endocrinol metabolism. 2013;305(3):E367–75. https://doi.org/10.1152/ajpendo.00644.2012.
14. Meurette O, Mehlen P. Notch Signaling in the Tumor Microenvironment. Cancer Cell. 2018;34(4):536–48. https://doi.org/10.1016/j.ccell.2018.07.009.
15. Porcheri C, Mitsiadis TA. Notch in Head and Neck Cancer. Adv Exp Med Biol. 2021;1287:81–103. https://doi.org/10.1007/978-3-030-55031-8_7.
16. Zhou B, Lin W, Long Y, Yang Y, Zhang H, Wu K, et al. Notch Signaling Pathway: Architecture, Disease, and Therapeutics. Signal Transduct Target therapy. 2022;7(1):95. https://doi.org/10.1038/s41392-022-00934-y.
17. Conery AR, Cao Y, Thompson EA, Townsend CM Jr., Ko TC, Luo K. Akt Interacts directly with Smad3 to Regulate the Sensitivity to TGF-Beta Induced Apoptosis. Nat Cell Biol. 2004;6(4):366–72. https://doi.org/10.1038/ncb1117.
18. Elyaman W, Bassil R, Bradshaw EM, Orent W, Lahoud Y, Zhu B, et al. Notch receptors and Smad3 signaling cooperate in the induction of interleukin-9-producing T cells. Immunity. 2012;36(4):623–34. https://doi.org/10.1016/j.immuni.2012.01.020.

Publisher's Note